ELSEVIER

PII: S1359-8368(96)00053-4

Composites Part B **28B** (1997) 523–534

1359-8368/97/$17.00

A refined higher-order composite box beam theory

Thomas R. McCarthy and Aditi Chattopadhyay
Department of Mechanical and Aerospace Engineering, Arizona State University, Tempe, AZ 85287-6106, USA
(Received 16 May 1996; accepted 20 September 1996)

A three-dimensional theory is developed to model composite box beams with arbitrary wall thicknesses. The theory, which is based on a refined displacement field, approximates the three-dimensional elasticity solution so that the beam cross-sectional properties are not reduced to one-dimensional beam parameters. Both in-plane and out-of-plane warping are included automatically in the formulation. The model can accurately capture the transverse shear stresses through the thickness of each wall while satisfying stress-free boundary conditions on the inner and outer surfaces of the beam. Numerical results are presented for beams with varying wall thicknesses and aspect ratios. The static results are correlated with available experimental data and show excellent agreement. Results presented for thick-walled box beams show the importance of including transverse shear in the formulation and the difficulty of defining a 'beam' twist for the entire cross-section. © 1997 Elsevier Science Limited.

(Keywords: B. mechanical properties; C. analytical modelling; composite box beams)

NOTATION

A_{ij}	zeroth-order laminate stiffness matrix (lb in^{-1})
B_{ij}	first-order laminate stiffness matrix (lb)
c	beam width (in)
D_{ij}	second-order laminate stiffness matrix (lb in)
d	beam height (in)
E_{ij}	third-order laminate stiffness matrix (lb in^{2})
$\mathbf{f}$	forcing vector (lb.)
F_{ij}	fourth-order laminate stiffness matrix (lb in^{3})
h	wall thickness (in)
H_{ij}	sixth-order laminate stiffness matrix (lb in^{5})
$\mathbf{K}$	stiffness matrix (lb in^{-1})
L	beam length (in)
$\mathbf{M}$	mass matrix (slugs)
$\mathbf{q}$	nodal degree-of-freedom vector
Q_{ij}	constitutive matrix (psi)
$\mathbf{S}$	nodal displacement relationship matrix
T	kinetic energy (lb in)
$\hat{t}_1, \hat{t}_2, \hat{t}_3$	applied surface tractions (lb in^{-2})
U	strain energy (lb in)
u_1, u_2, u_3	local displacements (in)
U_0	strain energy density (psi)
u_0, v_0, w_0	displacements at midplane of walls (in)
W_e	applied external work (lb in)
$\mathcal{X}_1, \mathcal{X}_2, \mathcal{X}_3$	body forces (lb in^{-3})
x, y, z	global coordinate system
$\boldsymbol{\beta}$	nodal strain relationship matrix
χ, η, ζ	local coordinate system
ε	strain tensor
ε^0	zeroth-order strain tensor
κ^0, κ^2	higher-order strain tensors (in^{-1} and in^{-2})
σ	stress tensor (psi)
ψ_x, ψ_y	higher-order displacement functions (rad)

INTRODUCTION

Composite materials are becoming increasingly popular for use as structural members in aircraft applications. Owing to the high strength-to-weight ratio offered by composites, structural weight is much less of an issue than it is for isotropic materials. Therefore it is no longer necessary to use thin-walled sections to model the load-carrying sections. Thus, it is essential to develop a general framework for the comprehensive analysis of such composite structures of arbitrary wall thickness.

Beam theories associated with isotropic materials have been well understood for years and these theories tend to predict the structural and dynamic response quite accurately[1]. Recently research has also been reported in deriving composite beam theories[2–10]. Among these, the more comprehensive anisotropic theories rely on a full three-dimensional finite element solution which can become very computationally intensive[1,2]. Wörndle[4] addresses comprehensive modeling of beams with solid cross-sections by using a full three-dimensional finite element solution technique. In [5], a comprehensive finite element method based on the variational asymptotical approach is used to model beams of arbitrary cross-sections. The theory includes warping terms, in addition to the extension and rotations of the beam, in which the average contribution of the warping over the cross-section of the beam is assumed to be zero. In the variational asymptotical

approach, the three-dimensional properties of the beam are reduced to one-dimensional beam properties (extension, twist and two bending terms) and the beam response is then approximated on the basis of a one-dimensional analysis. Results presented for thin-walled composite beams with this technique show very good correlation.

In other analysis of closed sections[6–10], as well as in some of the three-dimensional finite element models[2], the classical laminate theory (CLT) is used to model the individual plate elements of each beam. This theory, which neglects transverse shear effects, is only appropriate for thin laminates. However, as shown by Gu and Chattopadhyay[11], in the case of anisotropic material, the changes in interlaminar stiffnesses lead to transverse shear stresses even for "so-called" thin laminates.

The objective of this research is to develop a more general, but computationally efficient, theory for the adequate analysis of composite box beam sections with moderately thick walls. A refined higher-order displacement field is used to represent accurately the transverse shear stress distribution in composite laminates of arbitrary thickness. On the basis of this, a procedure is developed for the analysis of moderately thick-walled rectangular composite box beam sections with pretwist, taper and sweep to model load-carrying structural members used in aerospace applications. Unlike the beam theory described in [5], the proposed theory approximates the three-dimensional elasticity solution rather than reducing the beam properties to one-dimensional quantities. Further, the warping of the cross-section in this theory is determined such that stress-free boundary conditions are exactly satisfied on the inner and the outer surfaces.

PROBLEM FORMULATION

A single-celled composite box beam analysis is developed by using a higher-order composite laminate theory[12] which accounts for the distributions of shear strains through the thicknesses of each wall. Individual displacement fields are assumed for each of the four box beam walls (*Figure 1*). Continuity between the displacement fields is enforced at each of the four corners throughout the thickness of each plate. By using the higher-order laminate theory in each wall, the solution of cross-sectional deformations are an approximation of the three-dimensional exact elasticity approach. In this regard, the standard beam degrees of freedom (extension, twist and two bending terms) are not used. However, the three-dimensional cross-sectional deformation of the beam is fully described by stretching, bending, twisting, shearing and both in-plane and out-of-plane warping. Since the analysis is capable of modeling composite box beams of moderately large thicknesses, the model will accurately describe moderately thick-walled load-carrying members currently being used in aerospace applications. The procedure is developed for beams of short aspect ratio; therefore, by using a two-dimensional finite element model, the beam is discretized with unequal element sizes to describe accurately arbitrary spanwise distributions.

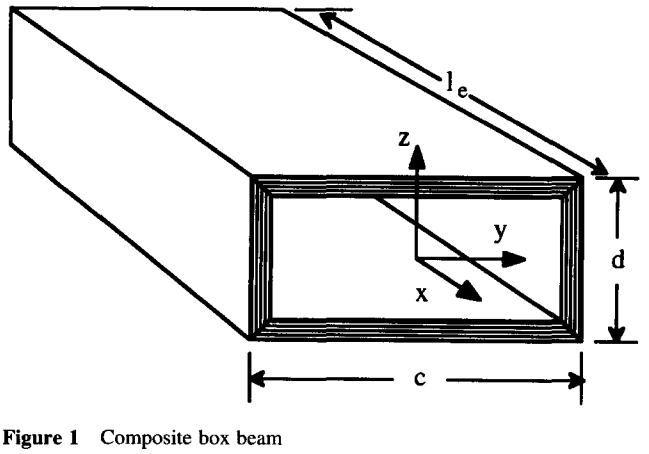

Figure 1 Composite box beam

COMPOSITE STRUCTURAL MODELING

The box beam is modeled by composite laminates representing the four walls (*Figure 1*). Several different coordinate systems are used throughout this paper and are defined as follows. The global coordinate system (x, y, z) is defined on the beam centroid (*Figure 1*). There are also coordinate systems which are defined locally in each wall of the box beam. The local coordinate system of the ith wall is denoted by (χ_i, η_i, ζ_i) as depicted in *Figure 2*.

Higher-order theory

The displacement field for each wall is defined in the local coordinate system (χ, η, ζ) as follows, where the subscript 'i' has been omitted for convenience throughout the remainder of the paper.

$$u_1(\chi,\eta,\zeta)=u_0(\chi,\eta)+\zeta\left(-\frac{\partial u_3(x,\eta)}{\partial\chi}+\psi_x(\chi,\eta)\right)+\zeta^2\phi_x(\chi,\eta)+\zeta\gamma_x(\chi,\eta) \tag{1a}$$

$$u_2(\chi,\eta,\zeta)=v_0(\chi,\eta)+\zeta\left(-\frac{\partial u_3(\chi,\eta)}{\partial\eta}+\psi_y(\chi,\eta)\right)+\zeta^2\phi_y(\chi,\eta)+\zeta\gamma_y(\chi,\eta) \tag{1b}$$

$$u_3(\chi,\eta)=w_0(\chi,\eta) \tag{1c}$$

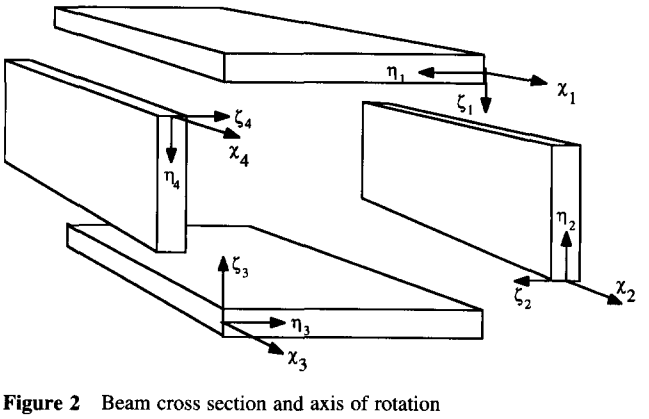

Figure 2 Beam cross section and axis of rotation

where u_0, v_0 and w_0 represent the displacements at the midplane of each plate and ψ_x and ψ_y represent the rotations of the normals to the midplane. The beam warping in each plate is represented by the functions ϕ_x, ϕ_y, γ_x and γ_y.

Boundary conditions

The higher-order functions (ϕ_x, ϕ_y, γ_x and γ_y) are determined on the basis of the condition that the transverse shear stresses, $\sigma_{\chi\zeta}$ and $\sigma_{\eta\zeta}$, vanish on the inner and outer surfaces of the beam. For composite laminates made up of layers of orthotropic lamina, this is equivalent to the requirement that the corresponding strains be zero on these surfaces. By using the stress-free boundary conditions, it can be shown that the original displacement field [eqn (1)] is reduced to the following set of equations:

$$u_1 = u_0 + \zeta\left(-\frac{\partial w_0}{\partial \chi} + \psi_x\right) - \frac{4}{3h^2}\zeta^3\psi_x \tag{2a}$$

$$u_2 = v_0 + \zeta\left(-\frac{\partial w_0}{\partial \eta} + \psi_y\right) - \frac{4}{3h^2}\zeta^3\psi_y \tag{2b}$$

$$u_3 = w_0 \tag{2c}$$

where the functions u_0, v_0, w_0, ψ_x and ψ_y represent unknown functions of χ and η.

Stress–strain relations

Owing to the fact that the stress and strain tensors are symmetric there are only six unique values of these quantities. Therefore, the following notation is used to define the stress and strain tensors in the local coordinate system:

$$\begin{Bmatrix}\sigma_1\\ \sigma_2\\ \sigma_3\\ \sigma_4\\ \sigma_5\\ \sigma_6\end{Bmatrix}^{\mathrm{T}} = \begin{Bmatrix}\sigma_{\chi\chi}\\ \sigma_{\eta\eta}\\ \sigma_{\zeta\zeta}\\ \sigma_{\eta\zeta}\\ \sigma_{\chi\zeta}\\ \sigma_{\chi\eta}\end{Bmatrix}^{\mathrm{T}} \quad \text{and} \quad \begin{Bmatrix}\varepsilon_1\\ \varepsilon_2\\ \varepsilon_3\\ \varepsilon_4\\ \varepsilon_5\\ \varepsilon_6\end{Bmatrix}^{\mathrm{T}} = \begin{Bmatrix}\varepsilon_{\chi\chi}\\ \varepsilon_{\eta\eta}\\ \varepsilon_{\zeta\zeta}\\ 2\varepsilon_{\eta\zeta}\\ 2\varepsilon_{\chi\zeta}\\ 2\varepsilon_{\chi\eta}\end{Bmatrix}^{\mathrm{T}} \tag{3a,b}$$

The generalized Hooke's law is used to relate the stress and strain. Assuming the products of the derivatives of the displacements to be small in the strain formulation, the local in-plane strains in the absence of pretwist are derived as follows:

$$\varepsilon_1 = \varepsilon_1^0 + \zeta\kappa_1^0 + \zeta^3\kappa_1^2 \tag{4a}$$

$$\varepsilon_2 = \varepsilon_2^0 + \zeta\kappa_2^0 + \zeta^3\kappa_2^2 \tag{4b}$$

$$\varepsilon_6 = \varepsilon_6^0 + \zeta\kappa_6^0 + \zeta^3\kappa_6^2 \tag{4c}$$

The out-of-plane strains are expressed similarly as:

$$\varepsilon_3 = 0 \tag{4d}$$

$$\varepsilon_4 = \varepsilon_4^0 + \zeta^2\kappa_4^2 \tag{4e}$$

$$\varepsilon_5 = \varepsilon_5^0 + \zeta^2\kappa_5^2 \tag{4f}$$

where the individual strain components are described in Appendix A.

Energy formulation

The beam equations of motion are derived by using Hamilton's principle[13] which assumes the following form:

$$\delta\int_{t_1}^{t_2}\left(U - T - W_{\mathrm{e}}\right)\mathrm{d}t = 0 \tag{5}$$

where $\delta(\ )$ represents the variation of $(\ )$ and U, T and W_{e} represent the total beam strain energy, kinetic energy and external work, respectively. By using variational principles, eqn (5) may be rewritten in terms of the individual plate quantities as follows:

$$\int_{t_1}^{t_2}\left(\sum_{i=1}^{N}\delta U_i - \delta T_i - \delta W_{\mathrm{e}_i}\right)\mathrm{d}t = 0 \tag{6}$$

where N is the total number of walls ($N = 4$ for a box beam). The individual strain energy density (U_0) in each plate is calculated as follows:

$$U_0 = \int_0^{\varepsilon_i}\sigma_i\,\mathrm{d}\varepsilon_i = \int_0^{\varepsilon_i}Q_{ij}\varepsilon_j\,\mathrm{d}\varepsilon_i = \frac{1}{2}Q_{ij}\varepsilon_i\varepsilon_j \tag{7}$$

where repeated indices ($i,j = 1,2,\ldots,6$) indicate summation, σ_i is the strain tensor and Q_{ij} are the full three-dimensional material properties in the local coordinate system. The total strain energy of the ith wall (U_i) is then written as

$$U_i = \int_V U_{0_i}\,\mathrm{d}V = \frac{1}{2}\int_V \varepsilon_m Q_{mn}\varepsilon_n\,\mathrm{d}V \tag{8}$$

where V indicates integration over the volume of the wall. The strain energy can be rewritten by using eqn (4) and (8) as:

$$U_i = \frac{1}{2}\int_\Omega \left\{\varepsilon_i^0\ \kappa_i^0\ \kappa_i^2\right\}\begin{bmatrix}A_{ij} & B_{ij} & E_{ij}\\ B_{ij} & D_{ij} & F_{ij}\\ E_{ij} & F_{ij} & H_{ij}\end{bmatrix}\begin{Bmatrix}\varepsilon_j^0\\ \kappa_j^0\\ \kappa_j^2\end{Bmatrix}\mathrm{d}\Omega + \frac{1}{2}\int_\Omega\left\{\varepsilon_m^0\ \kappa_m^2\right\}\begin{bmatrix}A_{mn} & D_{mn}\\ D_{mn} & F_{mn}\end{bmatrix}\begin{Bmatrix}\varepsilon_n^0\\ \kappa_n^2\end{Bmatrix}\mathrm{d}\Omega,$$

$$i,j = 1,2,6 \text{ and } m,n = 4,5 \tag{9}$$

where $\mathrm{d}\Omega$ is the differential area ($\mathrm{d}\Omega = \mathrm{d}\chi\mathrm{d}\eta$) and the laminate stiffness matrices (**A**–**H**) are defined in each of the walls as follows:

$$\left(A_{mn}, B_{mn}, D_{mn}, E_{mn}, F_{mn}, H_{mn}\right) = \int_{-h/2}^{h/2}Q_{mn}\left(1, z, z^2, z^3, z^4, z^6\right)\mathrm{d}\zeta \tag{10}$$

The external work due to applied loads and body forces (W_{e}) in the ith wall is written as

$$W_{\mathrm{e}_i} = \int_V \mathcal{X}_j u_j\,\mathrm{d}V + \int_S \hat{t}_j u_j\,\mathrm{d}S, \quad j = 1,2,3 \tag{11}$$

where u_j is the displacement vector defined as $[u\ v\ \mathrm{w}]^{\mathrm{T}}$; $\mathcal{X}_1$, $\mathcal{X}_2$ and $\mathcal{X}_3$ are the body forces in the x, y and z directions, respectively; and V represents the volume of the wall.

Applied surface tractions over the region of the surface S are denoted $\hat{t}_1$, $\hat{t}_2$ and $\hat{t}_3$ along the respective directions. The total kinetic energy of the beam is expressed as:

$$T_i = \frac{1}{2}\int_V \rho v_j v_j \, dV, \quad j = 1,2,3 \tag{12}$$

where $\mathbf{v}$ is the velocity vector defined as

$$\mathbf{v} = [\dot{u}\ \dot{v}\ \dot{w}]^T \tag{13}$$

and the notation $(\dot{})$ denotes a derivative with respect to time.

Variational method

The variation of strain energy is written as follows:

$$\delta U_i = \int_\Omega \{\varepsilon_i^0\ \kappa_i^0\ \kappa_i^2\} \begin{bmatrix} A_{ij} & B_{ij} & E_{ij} \\ B_{ij} & D_{ij} & F_{ij} \\ E_{ij} & F_{ij} & H_{ij} \end{bmatrix} \begin{Bmatrix} \delta\varepsilon_j^0 \\ \delta\kappa_j^0 \\ \delta\kappa_j^2 \end{Bmatrix} d\Omega + \int_\Omega \{\varepsilon_m^0\ \kappa_m^2\} \begin{bmatrix} A_{mn} & D_{mn} \\ D_{mn} & F_{mn} \end{bmatrix} \begin{Bmatrix} \delta\varepsilon_n^0 \\ \delta\kappa_n^2 \end{Bmatrix} d\Omega,$$

$$i,j = 1,2,6 \text{ and } m,n = 4,5 \tag{14}$$

The variation of the potential energy of the applied loads is:

$$\delta W_{e_i} = \int_V \hat{X}_j \delta u_j \, dV + \int_S \hat{t}_j \delta u_j \, dS, \quad j = 1,2,3 \tag{15}$$

Finally, the variation of the kinetic energy is written as:

$$\delta T_i = \int_V \rho v_j \delta v_j \, dV, \quad j = 1,2,3 \tag{16}$$

SOLUTION PROCEDURE

The equations of motion are discretized by using a two-dimensional finite element formulation in the local coordinate system of *each* individual plate (χ, η, ζ). A four-noded plate element is used to discretize the individual plates of the beam. This element is C^1 continuous in the zeroth-order displacements (u_0, v_0, w_0) and is C^0 continuous for the higher-order terms (ψ_x, ψ_y). As a result, the element contains 11 degrees of freedom per node which are defined in terms of the nodal degree of freedom vector as follows:

$$\tilde{\mathbf{q}} = \left[u_0, \frac{\partial u_0}{\partial \chi}, \frac{\partial u_0}{\partial \eta}, v_0, \frac{\partial v_0}{\partial \chi}, \frac{\partial v_0}{\partial \eta}, w_0, \frac{\partial w_0}{\partial \chi}, \frac{\partial w_0}{\partial \eta}, \psi_x, \psi_y\right]^T \tag{17}$$

Continuity conditions

To maintain the continuity of displacements throughout the entire beam, constraints are imposed at the comers of each individual plate as follows:

$${}^1u_0(\chi, \eta = b_1) = {}^2u_0(\chi, \eta = 0) \tag{18a}$$

$${}^1v_0(\chi, \eta = b_1) = -{}^2w_0(\chi, \eta = 0) \tag{18b}$$

$${}^1w_0(\chi, \eta = b_1) = {}^2v_0(\chi, \eta = 0) \tag{18c}$$

where the preceding superscripts '1' and '2' denote walls 1 and 2, respectively, and b_1 is the width of wall 1. It must be noted that these equalities are valid for all x and therefore the partial derivatives of the above equalities, with respect to x, also represent constraints. To ensure that the walls remain perpendicular to each other after deformation, the following constraints are imposed on the rotations about the χ-axis:

$${}^1w_{0,\eta}(\chi, \eta = b_1) = {}^2w_{0,\eta}(\chi, \eta = 0) \tag{19a}$$

$${}^1\psi_y(\chi, \eta = b_1) = {}^2\psi_y(\chi, \eta = 0) \tag{19b}$$

Similar sets of constraints are derived at each of the four comers of the beam cross-section.

Finite element formulation

The finite element approach is used to solve the complete beam equations of motion [eqn (6)]. Denoting $\mathbf{q}$ as the nodal degree-of-freedom vector, it is possible to express the strain [eqn (4)] in the following form:

$$\varepsilon_i = \beta_{ij} q_j, \quad i = 1,2,\ldots,6 \text{ and } j = 1,2,\ldots,\text{NDOF} \tag{20}$$

where NDOF is the total number of degrees of freedom. The partial derivatives of the strain with respect to q_j are then written as

$$\frac{\partial \varepsilon_i}{\partial q_j} = \beta_{ij} \tag{21}$$

Note that the matrix $\boldsymbol{\beta}$ can be expanded in terms of ζ as follows

$$\beta_{ij} = [\beta_{ij}^0\ \beta_{ij}^1\ \beta_{ij}^2\ \beta_{ij}^3] \cdot \{1\ \zeta\ \zeta^2\ \zeta^3\} \tag{22}$$

Similarly, the displacement vector $\mathbf{u}$ may be written as

$$u_i = S_{ij} q_j, \quad i = 1,2,3 \text{ and } j = 1,2,\ldots,\text{NDOF} \tag{23}$$

such that partial derivatives of the displacements with respect to q_j are as follows

$$\frac{\partial u_i}{\partial q_j} = S_{ij} \tag{24}$$

By using the above relationships, the beam equations of motion are written in matrix form as:

$$\mathbf{M}\ddot{\mathbf{q}} + \mathbf{K}\mathbf{q} = \mathbf{f} \tag{25}$$

where the mass and stiffness matrices are denoted

$$\mathbf{M} = \sum_{i=1}^{N} \left[\int_\Omega \rho \mathbf{S}^T \mathbf{S} \, d\Omega\right] \tag{26}$$

$$\mathbf{K} = \sum_{i=1}^{N} \left[\int_\Omega \mathcal{B}^T Q \mathcal{B} \, d\Omega\right] \tag{27}$$

and the forcing vector is

$$\mathbf{f} = \sum_{i=1}^{N} \left[\int_\Omega \mathbf{S}\hat{\mathbf{X}} \, d\Omega + \int_S \mathbf{S}\hat{\mathbf{t}} \, dS\right] \tag{28}$$

Results

To demonstrate the accuracy of the higher-order composite theory, results are presented first for an orthotropic plate for which an exact solution is available. Next, the results of the box beam analysis are verified by performing static correlation tests with available experimental results and other beam theories. Finally, results are presented for composite beams with thick-walled cross-sections.

Higher-order plate correlation

To show the importance of the shear terms in the individual plates and how well the present theory can capture them, results from a simply supported square, orthotropic plate under a uniform load are presented. The material properties of the plate are listed in *Table 1*. *Figure 3* shows the normalized center deflection of the plate for various plate thicknesses. The normal stress and the shear stress are shown in *Figure 4*. Note that, in *Figure 4*, results from the classical laminate theory (CLT) are not presented because in case of the normal stress, they are nearly identical to the results from the higher-order theory and, in case of the transverse shear stress, they are zero. From these figures, two important conclusions are drawn. First, the higher-order plate theory correlates extremely well with the exact elasticity solution[14]. Also, for moderately thick to very thick plates, the normal stress and the shear stress are significant and therefore CLT should not be used in such cases.

Table 1 Summary of orthotropic material properties[14]

E_1 ($\times 10^6$ psi)	20.83
E_2 ($\times 10^6$ psi)	1.094
G_{12} ($\times 10^6$ psi)	6.10
G_{13} ($\times 10^6$ psi)	3.71
μ_{12}	0.44

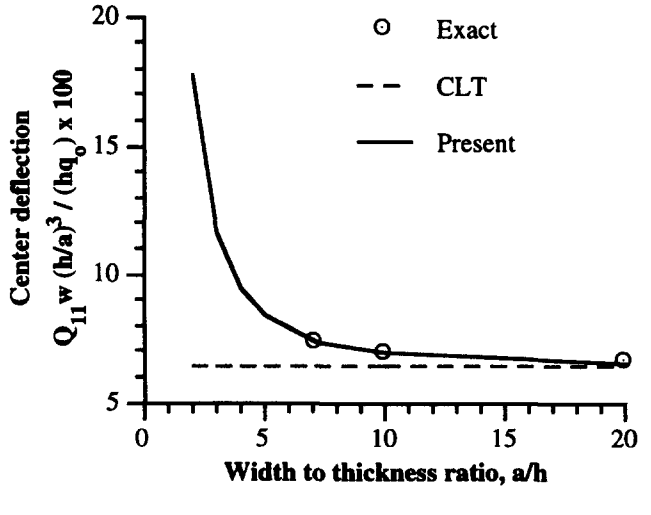

Figure 3 Normalized center deflection of fixed orthotropic square plate under uniform distributed load

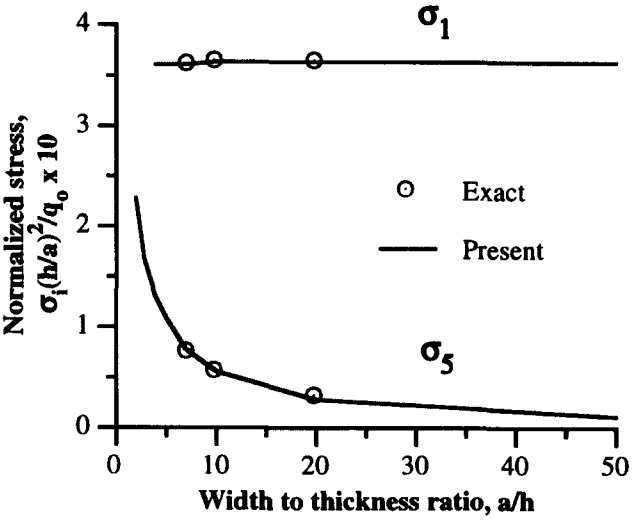

Figure 4 Normalized stresses of fixed orthotropic square plate under uniform distributed load

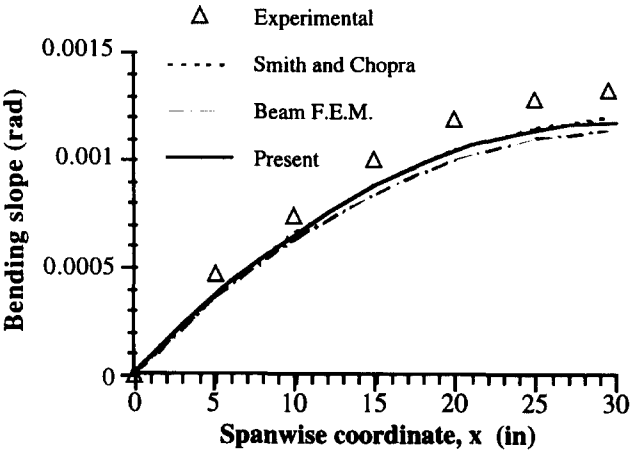

Figure 5 Bending slope of cross ply beam under 1 lb. tip bending load

Static results: thin-walled beams

To validate the developed procedure, correlations are made with available experimental results on a thin-walled box beam[14] and a previously developed analytical model[15]. The analytical model developed in [15] is a one-dimensional thin-walled beam model based on CLT in which the out-of-plane warping effects are based on a contour analysis. The details of the beams studied are presented in *Table 1*. The cross-ply and symmetric beams are all subjected to two different loading conditions: a 1 lb bending load at the tip and a 1 lb in tip moment. The antisymmetric beams are subjected to a 1 lb axial load at the tip and 1 lb in tip moment.

Cross-ply. The bending slope of the cross-ply beam under a 1 lb tip bending load is presented in *Figure 5*, which compares the experimental data[14], the results of the analytical model[15] and the results from the present study. Further results from a beam finite element model, which were reported in [15], are also presented. As mentioned in [15], this two-dimensional finite element technique is as accurate as a full three-dimensional finite element model for the

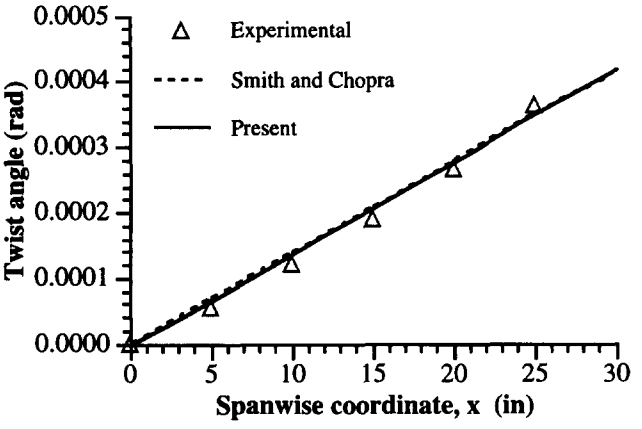

Figure 6 Twist angle of cross ply beam under 1 lb.-in. tip moment

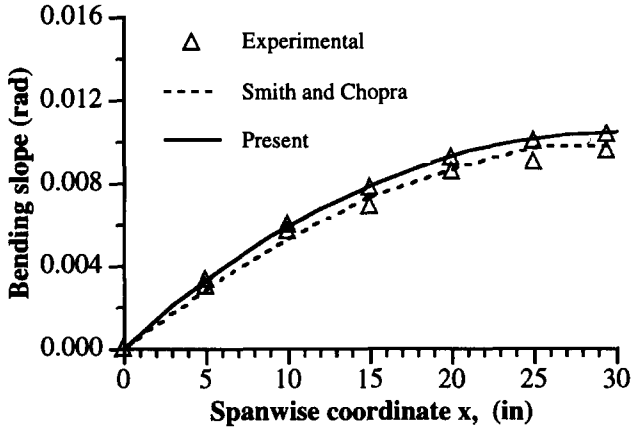

Figure 7 Bending slope of symmetric 15° beam under 1 lb. tip bending load

particular beams studied in this paper. From *Figure 5*, it is seen that all three modeling techniques underpredict the bending slope of the cross-ply beam. This can be attributed to fiber alignment problems that are typically encountered during fabrication and curing of the beam. A slight shift from the desired 0° and 90° ply orientation can introduce additional coupling terms which will reduce bending stiffnesses, thereby increasing the bending slope. Overall, there is still good correlation between all three modeling techniques in this case. The twist angle of the cross-ply beam due to a 1 lb in tip moment is shown in *Figure 6* and excellent correlation is observed for both the analytical model[15] and the present approach.

Symmetric beams. The bending slope of the symmetric 15° beam under a 1 lb tip bending load is presented in *Figure 7*, where good correlation is observed for both modeling techniques. There are two sets of experimental data presented in this figure owing to the fact that two separate beams were tested in [14]. The induced twist due to tip bending load is presented in *Figure 8*, which shows that the present approach slightly overpredicts the twist angle at the tip compared with the analytical model of [15]. Overall, however, there is good correlation with the experimental data for both models.

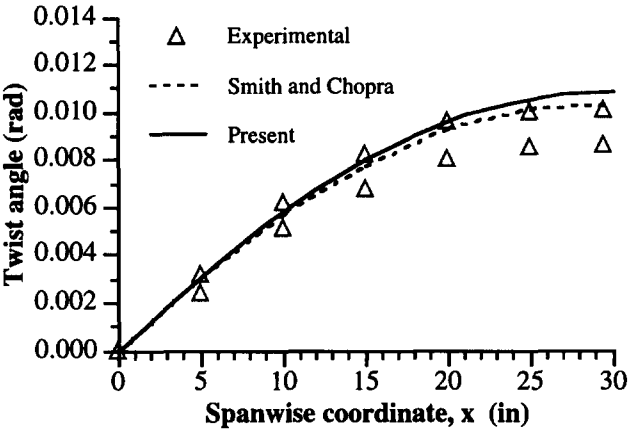

Figure 8 Bending induced twist of symmetric 15° beam under 1 lb. tip bending load

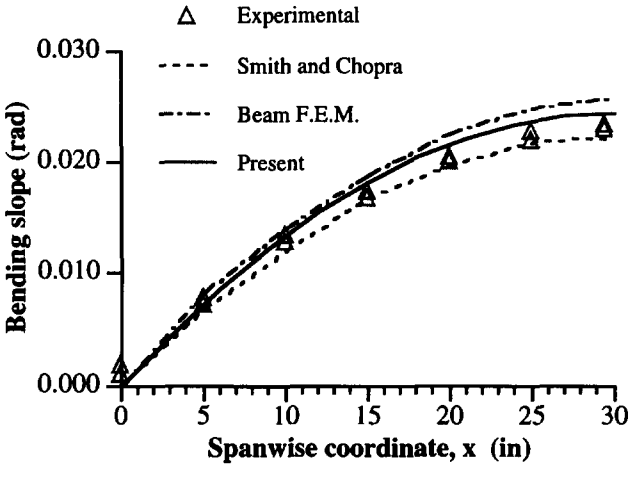

Figure 9 Bending slope of 30° symmetric beam under 1 lb. tip bending load

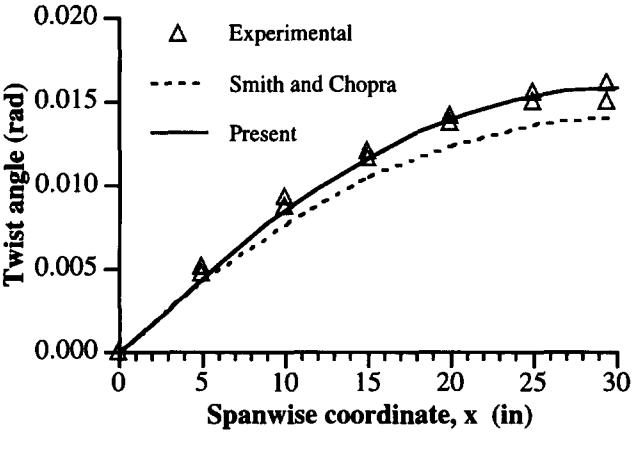

Figure 10 Bending induced twist of 30° symmetric beam under 1 lb. tip bending load

The bending slope of the symmetric 30° beam is presented in *Figure 9*. This figure also shows the results from the beam finite element method presented in [15]. From the figure it is observed that the analytical technique slightly underpredicts the behavior and the present approach slightly overpredicts the bending slope. The beam finite element

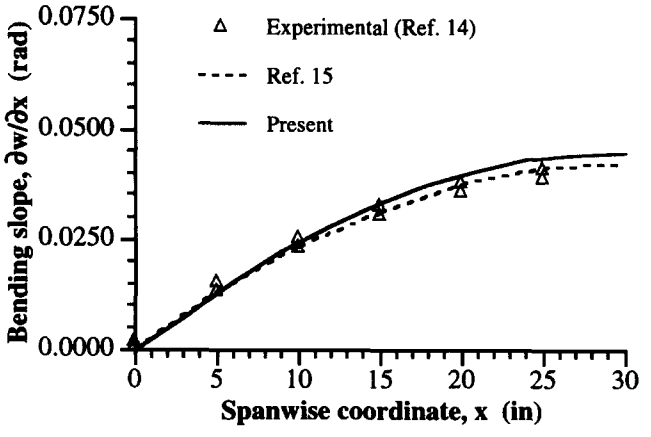

Figure 11 Bending slope of $[45°]_6$ thin-walled beam under 1 lb. bending load at tip

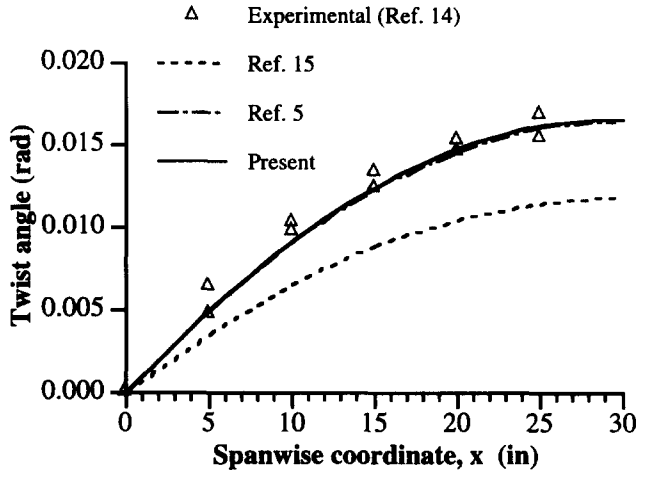

Figure 12 Bending induced twist of $[45°]_6$ thin-walled beam under 1 lb. bending load at tip

method[15] overpredicts the slope more significantly than the current approach. Once again, good correlation exists between all techniques. The induced twist due to bending load is presented in *Figure 10*. The analytical technique again underpredicts the response. The results from the present study correlate extremely well with the experimental data in this case.

The results from the symmetric 45° beam subjected to a 1 lb tip bending load are presented in *Figures 11* and *12*. As shown in *Figure 11*, the bending slope is slightly overpredicted by the present model although the correlation with experimental data is still very good. The analytical technique[15] also correlates well. In case of the induced twist due to the bending load, the trends are significantly different (*Figure 12*). The analytical method grossly underpredicts the twist in this case while the present approach correlates extremely well with the experimental data. Further, the results are in excellent agreement with the variational asymptotical approach of Cesnik *et al.*[5] which is well suited for this thin-walled box beam. This approach reduces the cross-sectional properties into one-dimensional beam properties based on an expansion in terms of a small parameter which is defined to be the ratio of the beam height

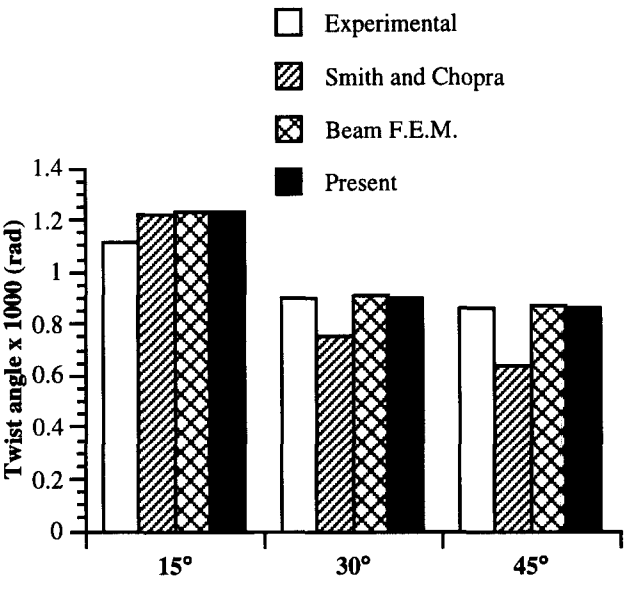

Figure 13 Twist at $x/R = 0.5$ for 1 lb in. tip moment of symmetric beams

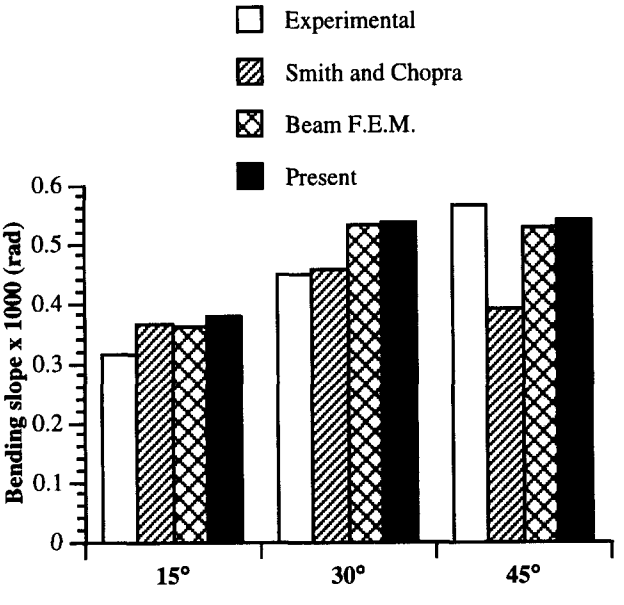

Figure 14 Bending slope at $x/R = 0.5$ for 1 lb in. tip moment of symmetric beams

and length. This theory does include both in-plane and out-of-plane warping.

The results from the 1 lb in. tip moment for all three symmetric beams are presented in *Figures 13* and *14*. Since the variation of the response is linear, only the results at the midspan location ($x/R = 0.5$) are presented. From *Figure 13* it is seen that there is scattered correlation with the experimental bending slope, but it must be noted that actual values of the slope are very small (of the order of 0.0005 rad). In case of the 15° symmetric beam, both the analytical and the present approach overpredict the slope as does the beam finite element method. In the case of the symmetric 30° beam, the present approach and the beam finite element method again overpredict the slope, whereas

Table 2 Details of composite beams[15,16]

	Flanges		Webs	
	Top	Bottom	Left	Right
Cross-ply	$[0°/90°]_3$	$[0°/90°]_3$	$[0°/90°]_3$	$[0°/90°]_3$
Symmetric 15°	$[15°]_6$	$[15°]_6$	$[15°/-15°]_3$	$[15°/-15°]_3$
Symmetric 30°	$[30°]_6$	$[30°]_6$	$[30°/-30°]_3$	$[30°/-30°]_3$
Symmetric 45°	$[45°]_6$	$[45°]_6$	$[45°/-15°]_3$	$[45°/-45°]_3$
Antisymmetric 15°	$[15°]_6$	$[-15°]_6$	$[15°]_6$	$[-15°]_6$
Antisymmetric 30°	$[0°/30°]_3$	$[0°/-30°]_3$	$[0°/30°]_3$	$[0°/-30°]_3$
Antisymmetric 45°	$[0°/45°]_3$	$[0°/-45°]_3$	$[0°/45°]_3$	$[0°/-45°]_3$

Length = 30 in, width = 0.953 in, depth = 0.53 in, ply thickness = 0.005 in, number of plies = 6, wall thickness = 0.030 in. Mechanical properties: $E_L = 20.59 \times 10^6$ psi, $E_T = 1.42 \times 10^6$ psi, $G_{LT} = 0.89 \times 10^6$ psi, $\nu_{LT} = 0.42$ (cross-ply dimensions: width = 2.06 in, depth = 1.025 in)

the analytical method[15] correlates well with the experimental data. Finally, in the case of the symmetric 45° beam, the analytical method greatly underpredicts the slope whereas the beam finite element method and the present approach correlate very well. Overall, however, there is good correlation with the experimental data for all three techniques, especially when the actual magnitude of the slope is taken into consideration. The twist angles are presented in *Figure 14*. In the case of the symmetric 15° beam, all three techniques show overprediction of the twist angle. However, for the symmetric 30° beam and the symmetric 45° beam, both the present approach and the beam finite element method correlate extremely well with the experimental data while the analytical technique significantly underpredicts the behavior.

By examining *Figures 5–14*, it is observed that analytical model of [15] correlates well with experimental data for the cross-ply beam and the 15° symmetric beam. In hte case of the 30° symmetric beam, the analytical model begins to underpredict the behavior. This is particularly evident in *Figure 8*, which presents the induced twist due to a 1 lb tip bending load. The analytical method greatly underpredicts the behavior of the symmetric 45° beam for all cases studied, except the bending slope due to the 1 lb tip bending load. It is also observed from these figures that although the present approach slightly overpredicts the beam behavior for the lower angle plies, the present technique correlates very well with the experimental data for all cases, especially in cases with large ply orientations. Further, in cases where the present approach does overpredict the behavior of the beam, the beam finite element method[15] shows the same trend (*Figures 7, 13* and *14*).

Antisymmetric beams. The results from the three antisymmetric beams (*Table 2*) are presented in *Figures 15* and *16*. Again, since the response is linear, only the results at the midspan location are presented. As in *Figures 13* and *14*, the actual magnitude of the twist angle must be noted in these figures. The twist angle due to a 1 lb in tip moment is seen in *Figure 15*. In the case of the 15° antisymmetric beam, the analytical model, the beam finite element method and the present approach all correlate very well with the experimental data. For the other two antisymmetric beams, all three approaches show similar trends, slightly underpredicting the response compared with the experimental results. Similar trends are observed in *Figure 14*, which presents the twist

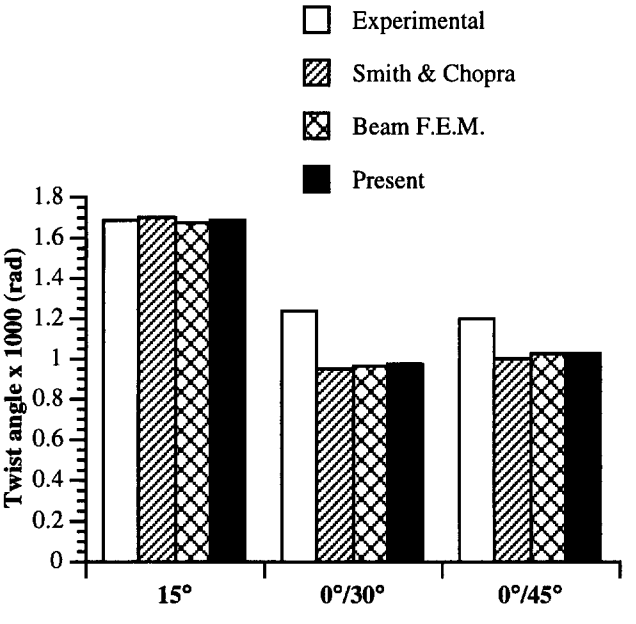

Figure 15 Twist at $x/R = 0.5$ for 1 lb in. tip moment of anti-symmetric beams

angle for a 1 lb axial tip load. For the antisymmetric 15° beam all three approaches slightly overpredict the twist. However, all three approaches predict the behavior very well for the antisymmetric 30° beam and the antisymmetric 45° beam.

Overall, both the analytical model of [15] and the present approach correlate well with the experimental data for the antisymmetric beams. Both techniques predict the same trends for all three beams. The results from the present approach are slightly better than the analytical results for the antisymmetric 15° beam.

Static results: thick-walled beams

To demonstrate the importance of including transverse shear in the beam formulation, results are now presented for a series of thick-walled beams. Because of the lack of available experimental data, only analytical results are presented. Two different composite lay-ups are used which correspond to the symmetric 15° beam and the symmetric 45° beam (*Table 2*). The beams studied have a length-to-width ratio (L/c) of 2.5 and a width-to-height ratio of (c/d) of 2. Since the goal is to investigate the effects of thick-walled

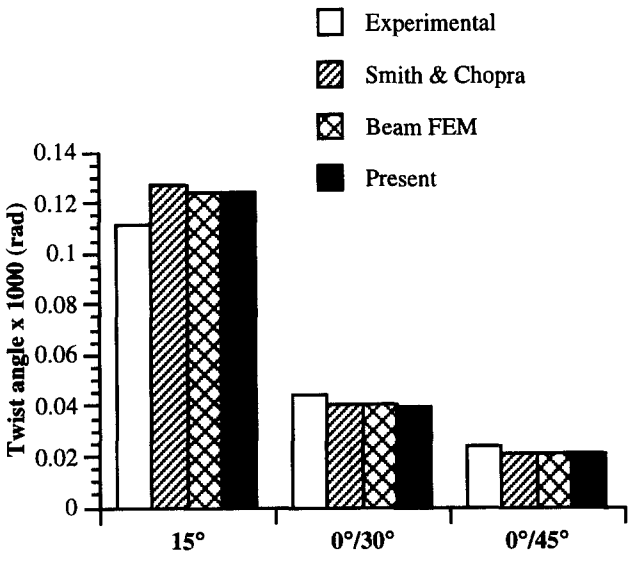

Figure 16 Bending slope at $x/R = 0.5$ for 1 lb in. tip axial load of symmetric beams

Table 3 Summary of thick-walled beam dimensions

L (in)	5.0
c (in)	2.0
d (in)	1.0
Wall thickness, h (in)	0.25

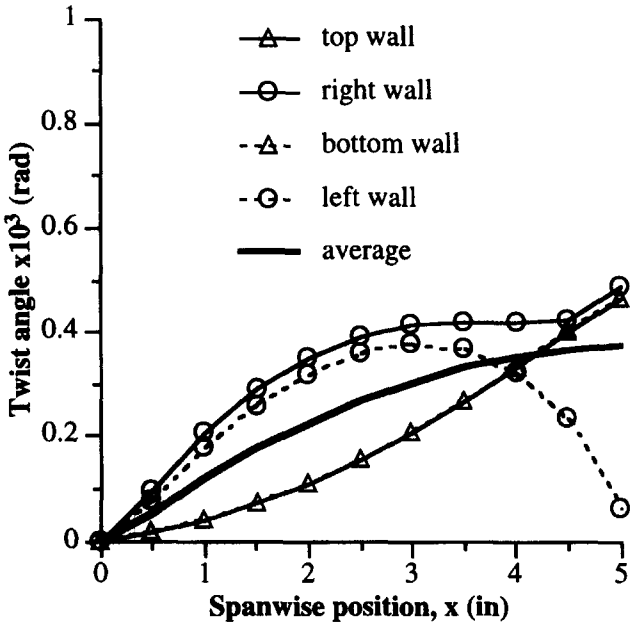

Figure 17 Bending induced twist of thick-walled 15° beam under 100 lb. tip bending load

beams, the wall thicknesses used in this study are 0.25 in. As a result, the width-to-thickness ratio (c/h) of the horizontal walls is 8 and the height-to-thickness ratio (d/h) of the vertical walls is 4 (*Table 3*). These two beam configurations are subjected to a 100 lb bending load at the tip as well as a 100 lb in. tip moment.

Figure 17 presents the elastic twist for the thick-walled 15° symmetric beam subjected to a tip bending load. From

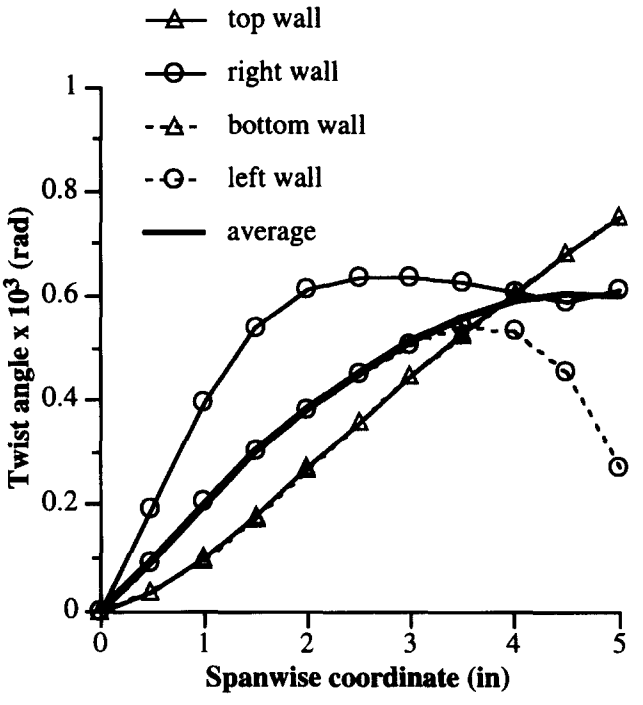

Figure 18 Bending induced twist of thick-walled 45° beam under 100 lb. tip bending load

the figure it is observed that, in addition to the fact that the local twist in the four individual walls is nonlinear, the average twist in each of the four walls is also nonlinear. This is different from the trends observed in the case of the thin-walled beams where the local twists in the individual walls are nearly identical and linear. In general, the local values of twist are very nearly linear for the thin-walled beams and further the values are very close to the average values, which are presented in *Figure 13*. Thus the average twist is a good representation of the beam twist for thin-walled beams. In the thick-walled case, however, the local twist differs significantly in the individual walls and as a result it is difficult to designate a value of 'beam twist' for the entire cross-section. *Figure 17* also shows that the twist in the vertical walls are not equal to each other, while the twist in the horizontal walls are equal. This is due to the fact that the ply angles in the horizontal walls are all $+15°$ and the two opposite walls are mirror images of each other. In the vertical walls, however, the stacking sequence in the opposite walls differs by a sign change (e.g. $\pm 15°$ in the right wall and $\mp 15°$ in the left wall). This nonlinear trend is more observable in *Figure 18*, which presents the induced twist of the symmetric 45° beam subjected to a tip bending load. The nonlinear behavior of the vertical walls is more dominant in this case.

A more complete explanation for this phenomenom is presented in *Figures 19* and *20*. *Figure 19(a)* shows how the tip bending load is applied to the individual walls of the beam. In *Figure 19(b)*, the resulting displacements for unconnected walls (that is, individual plates) is shown where it is seen that displacements in the horizontal walls are described by a translation and a rotation. This is due to the fact that the plies in these walls are all of the same value (e.g. $+45°$) and therefore the laminate is unbalanced. Since

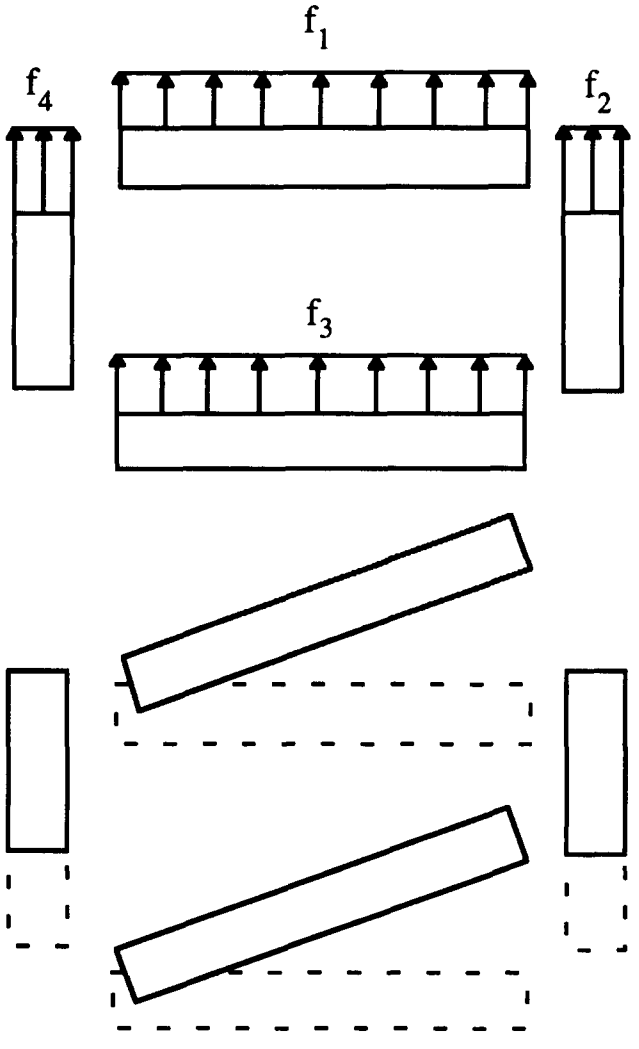

Figure 19 (a) Schematic of load distribution for tip bending load. (b) Form of individual wall displacements for tip bending load

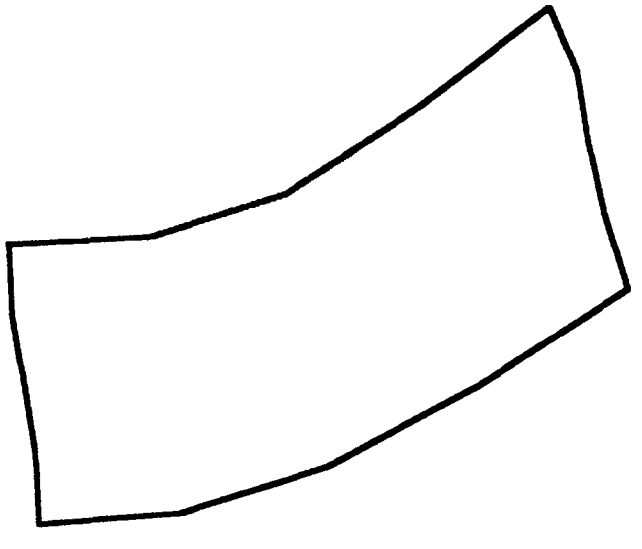

Figure 20 Deformation of cross section at tip due to tip bending load

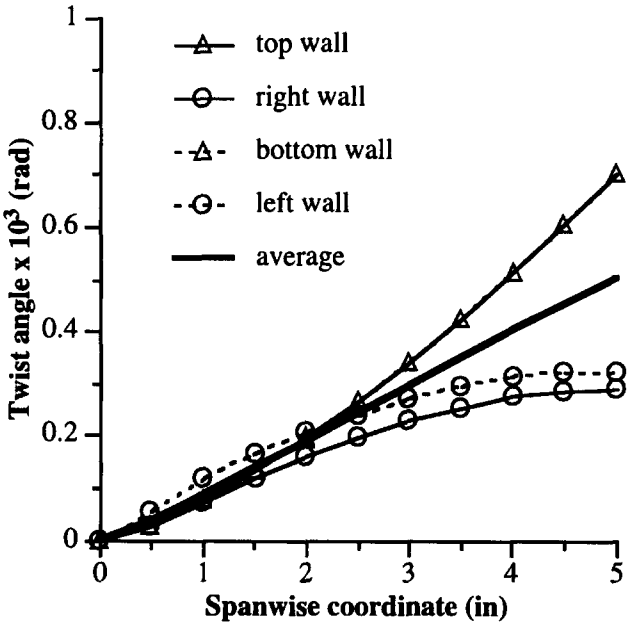

Figure 21 Twist of thick-walled 15° beam under 100 lb in. tip moment

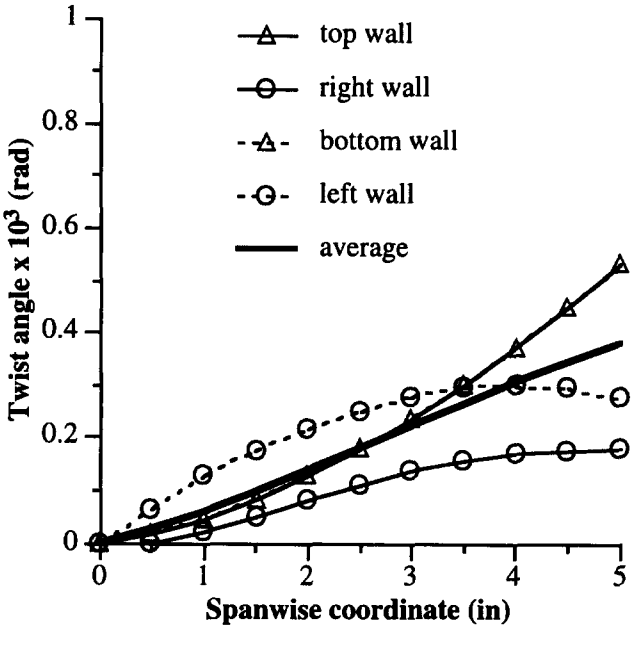

Figure 22 Twist of thick-walled 45° beam under 100 lb in. tip moment

both of the vertical walls are balanced (e.g. ± 45°) there is no rotation in these walls and the displacement is purely translational. From *Figure 19(b)* it is seen that the rotational displacement of the horizontal walls restricts the translational motion of the left vertical wall, whereas the rotational motion in the horizontal walls is complementary to the translational motion of the right wall. As a result, the horizontal walls become cambered which in turn induces large shearing stresses in the vertical walls. This type of bending behavior is shown in *Figure 20*, which presents the deformation (greatly magnified) of the tip cross-section for the 45° symmetric beam subjected to a tip bending load. The

shearing of the vertical walls and the cambering of the horizontal walls is seen from this figure.

The twist angle due to a 100 lb in tip moment for the 15° symmetric, thick-walled beam is presented in *Figure 21*. Similar trends to those obtained with the tip bending load are observed. In this case, however, the average twist of all four individual walls is very nearly linear. By comparison, in the case of the thin-walled, symmetric 15° beam, the twist angle due to a 1 lb in. tip moment is linear in each of the four walls, except at the tip where the values are slightly larger for the horizontal walls compared with the vertical walls. The trend of the thick-walled beams is more observable in *Figure 22*, which shows the twist angle of the thick-walled, 45° symmetric beam due to a 100 lb in tip moment.

The results presented indicate the importance of including transverse shear effects in the beam formulation. Further, the results also show that, in general, the twist of a composite beam is a local quantity which can be defined only locally, at a point. The definition of the twist at the centroid of a beam (or some other arbitrary point) is an approximation which, in the case of thick-walled sections, can be erroneous.

CONCLUDING REMARKS

A new beam theory has been developed to model composite box beams with arbitrary wall thicknesses. The theory, which is based on higher-order composite laminate theory, approximates the three-dimensional elasticity solution rather than reducing the cross-sectional properties to one-dimensional beam properties. The developed theory automatically satisfies the stress-free boundary conditions on the inner and outer surfaces of the beam. Both in-plane and out-of-plane warping are included in the formulation. The following important observations are made.

(1) Very good overall agreement is observed between the static results and available experimental data for thin-walled beams.
(2) For large angle-ply laminates (e.g. 45°), the present approach predicts the behavior very well, and represents a significant improvement over a previously developed analytical method.
(3) The results from the symmetric beams have better overall correlation than those from the antisymmetric beams. This is probably due to the fact that the magnitude of the twist measured for the antisymmetric beam correlation is very small.
(4) The effect of transverse shear stresses is critical in the case of thick-walled sections. This introduces large nonlinearities in the twist distribution. Further, the local twists in the individual walls are not equal as is the case for the thin-walled beams.
(5) The 'beam' twist is a local quantity which can only be defined at a point in the cross-section. Arbitrarily defining the twist at a convenient point in the beam cross-section is inaccurate for thick-walled cross-sections.

ACKNOWLEDGEMENTS

The authors would like to acknowledge support of this work through a grant from the NASA Ames Research Center, grant number NAG2-771, Technical Monitor Dr Sesi Kottapalli.

APPENDIX

A. Strain definitions

The zeroth-order in-plane strains in the absence of pretwist are defined as follows:

$$\begin{Bmatrix} \varepsilon_1^0 \\ \varepsilon_2^0 \\ \varepsilon_6^0 \end{Bmatrix} = \begin{Bmatrix} [u_{0,\chi}] \\ v_{0,\eta} \\ u_{0,\eta} + v_{0,\chi} \end{Bmatrix} \tag{A1}$$

The first-order in-plane strains are:

$$\begin{Bmatrix} \kappa_1^0 \\ \kappa_2^0 \\ \kappa_6^0 \end{Bmatrix} = \begin{Bmatrix} [-w_{0,\chi\chi} + \psi_{x,\chi}] \\ -w_{0,\eta\eta} + \psi_{y,\eta} \\ -2w_{0,\chi\eta} + \psi_{x,\eta} + \psi_{y,\chi} \end{Bmatrix} \tag{A2}$$

and the third components of the in-plane strain are:

$$\begin{Bmatrix} \kappa_1^2 \\ \kappa_2^2 \\ \kappa_6^2 \end{Bmatrix} = -\frac{4}{3h^2} \begin{Bmatrix} [\psi_{x,\chi}] \\ \psi_{y,\eta} \\ \psi_{x,\eta} + \psi_{y,\chi} \end{Bmatrix} \tag{A3}$$

The zeroth- and the second-order components of the out-of-plane strains are defined as follows:

$$\begin{Bmatrix} \varepsilon_4^0 \\ \varepsilon_5^0 \end{Bmatrix} = \begin{Bmatrix} \psi_y \\ \psi_x \end{Bmatrix} \tag{A4}$$

$$\begin{Bmatrix} \kappa_4^2 \\ \kappa_5^2 \end{Bmatrix} = -\frac{4}{h^2} \begin{Bmatrix} \psi_y \\ \psi_x \end{Bmatrix} \tag{A5}$$

REFERENCES

1 Hodges, D.H., Ormiston, R.A. and Peters, D.A. On the nonlinear deformation geometry of Euler–Bernoulli beams, NASA TP-1566, National Aeronautics and Space Administration, Washington, DC, April 1980.
2 Kosmatka, J.B. and Friedmann, P.P., Vibration analysis of composite turbopropellers using a Nonlinear Beam-Type Finite-Element Approach. *AIAA J.*, 1989, **27**(11), 1606–1614.
3 Stemple, A.D. and Lee, S.W., Finite-element model for composite beams with arbitrary cross-sectional warping. *AIAA J.*, 1988, **26**(12), 1512–1520.
4 Wörndle, R., Calculation of the cross section properties and the shear stresses of composite rotor blades. *Vertica*, 1982, **6**, 111–129.
5 Cesnik, C.E.S., Sutyrin, V.G. and Hodges, D.H. Refined theory of twisted and curved composite beams: the role of short-wavelength extrapolation. Paper No. AIAA 94-1451-CP in 'Proceedings of 35th Structures, Structural Dynamics, and Materials Conf.', Hilton Head, SC, 18–20 April 1994, pp. 1134–1143.
6 Bauchau, O.A., A beam theory for anisotropic materials. *J. Appl. Mech.*, 1985, **52**, 416–422.

7 Rand, O., Theoretical modeling of composite rotating beams. *Vertica*, 1990, **14**(3), 329–343.
8 Rehfield, L.W., Atilgan, A.R. and Hodges, D.H., Nonclassical behavior of thin-walled composite beams with closed cross sections. *J. Am. Helicopter Soc.*, 1990, **35**, 42–50.
9 Smith, E.C. and Chopra, I., Formulation and evaluation of an analytical model for composite box-beams. *J. Am. Helicopter Soc.*, 1991, **36**, 23–35.
10 Kalfon, J.P. and Rand, O. Nonlinear analysis of composite thin-walled helicopter blades. In 'Proc. 48th Annual Forum of the American Helicopter Society', Washington, DC, 1992, pp. 1465–1478.
11 Gu, H. and Chattopadhyay, A., A new higher order plate theory in modeling delamination buckling of composite laminates. *AIAA J.*, 1994, **32**(8), 1709–1716.
12 Reddy, J.N., A general non-linear third-order theory of plates with moderate thickness. *Int. J. Non-Linear Mech.*, 1990, **25**(6), 677–686.
13 Reddy, J.N. 'Energy and Variational Principles in Applied Mechanics', John Wiley and Sons, New York, 1984.
14 Chandra, R., Stemple, A.D. and Chopra, I., Thin-walled composite beams under bending, torsional and extensional loads. *J. Aircraft*, 1990, **27**(7), 619–626.
15 Smith, E.C. and Chopra, I., Formulation and evaluation of an analytical model for composite box-beams. *J. Am. Helicopter Soc.*, 1900, **36**(7), 23–35